THEORETICAL INVESTIGATION OF RECTANGULAR PATCH ANTENNA MINIATURIZATION BASED ON THE DPS-ENG BI-LAYER SUPER-SLOW TM WAVE

J. Xiong[1, *], **H. Li**[2], **B. Z. Wang**[1], **Y. Jin**[2], **and S. He**[2]

[1]Computational Electromagnetics Laboratory, Institute of Applied Physics, University of Electronic Science and Technology of China, Chengdu 610054, China

[2]Center for Optical and Electromagnetic Research (COER), Zhejiang University, Hangzhou 310058, China

Abstract—The TM_0 surface mode in an infinitely long parallel-plate waveguide filled with a double-positive (DPS) and epsilon-negative (ENG) metamaterial bi-layer is studied. With proper constitutive parameters and thicknesses of the two layers, the slow-wave factor (SWF) for such a parallel-plate waveguide can tend to infinity as the frequency decreases. A 2-D cavity based on the DPS-ENG bi-layer waveguide is constructed and studied to evaluate the radiation ability of its corresponding patch antenna. Based on the cavity model analysis of patch antennas, we show that good efficiency for broadside radiation of such a cavity-based rectangular patch antenna can be achieved when one layer of the cavity is shielded (or partially shielded) by PEC boundaries. Taking practical loss and dispersion into consideration, a miniaturized cavity-based rectangular patch antenna is proposed as an example. With the super-slow TM_0 surface mode excited in the bi-layer by a simple coaxial line feeding, the antenna has a dimension of only $0.107\lambda_0 \times 0.129\lambda_0 \times 0.045\lambda_0$. The patch antenna produces broadside radiation, and fairly good radiation efficiency is achieved. The PEC-Partially-Shielded-ENG-Cavity based rectangular patch antenna with a further miniaturization but reduced radiation efficiency is also discussed.

1. INTRODUCTION

Microstrip patch antennas have been considered as one of the most promising candidates in government, commercial and defense applications, due to their attractive advantages such as simplicity of the structure, low profile, light weight, easy fabrication, and excellent conformability with planar integrated circuits and even nonplanar surfaces [1, 2]. Due to the rapidly increasing constraints on the size of the radiator in modern telecommunication and defense applications such as satellites, aircrafts, missiles, and radars, there is an obvious demand for patch antennas with highly squeezed lateral size (below subwavelength and as small as possible) while other properties such as impedance matching, radiation pattern and polarization can be well maintained. Conventional miniaturization approaches include using a dielectric substrate of high permittivity, shorting wall or shorting pin loading (like the PIFAs), slot cut on the patch, or a combination of them [2–4]. However, such extent of size reduction is still limited and can not meet the requirement of some extremely compact antennas, and the above approaches can also bring some side effects such as strong surface wave, deterioration of radiation efficiency, shape of the radiation pattern, impedance bandwidth, etc..

In the past decade, electromagnetic metamaterials [5, 6] have attracted considerable attention, and extensive studies have been performed to design novel antennas with improved properties [7–11]. Particularly, metamaterials have been introduced and applied to shrink the size of patch antennas [12–20]. Itoh et al. have proposed a zeroth order resonating antenna with a composite right/left-handed (CRLH) transmission line [5, 12, 13]. Although the physical size of the antenna can be theoretically arbitrarily small at the zeroth order mode, it produces a monopolar radiation pattern rather than broadside radiation, and when the physical size of the antenna is reduced to certain extent, the equivalent out-of-phase magnetic currents along two opposite edges of the zeroth order resonating antenna get so close that they cancel each other, which thus inevitably renders poor radiation efficiency [13, 18]. Alternatively, people also use metamaterials with negative electromagnetic constitutive parameters, i.e., negative real part for only permittivity (ENG), negative real part for only permeability (MNG), and negative real parts for both permittivity and permeability (DNG) [6], to shrink the size of patch antennas. Based on the idea of phase compensation [16], rectangular, circular, elliptical and annular ring patch antennas on a juxtaposed DPS-ENG, DPS-MNG, or DPS-DNG pair have been investigated, and a series of effective subwavelength radiators have been proposed [17–

20], when the required radiation efficiency and radiation pattern are sufficiently taken into consideration. A dual-band rectangular patch antenna partially filled with MNG/DNG metamaterials with broadside radiation at both operating bands has also been proposed recently [21, 22].

The guided modes in a 2-D DNG-DPS or ENG-MNG parallel-plate waveguide have been theoretically discussed in [23–25]. One of the most interesting features of such waveguide is its super-slow surface mode with the slow-wave factor tending to infinity at low frequency. In this paper, we investigate theoretically the potential miniaturization of rectangular patch antennas with efficient broadside radiation, based on such super-slow surface mode. We will first show in Section 2 that the DNG layer of the DPS-DNG bi-layer parallel-plate waveguide considered in [23–25] can be replaced by an ENG layer, which is much easier to be implemented practically. Then in Section 3 we study a PEC-Shielded-ENG-Cavity (PSEC) and a PEC-Partially-Shielded-ENG-Cavity (PPSEC), formed by terminating the infinitely long parallel-plate waveguide with PMC or PMC-PEC hybrid boundaries. Theoretical and simulated results show that the PSEC and PPSEC can be applied to design a highly miniaturized rectangular patch antenna with efficient broadside radiation. In Section 4, a rectangular patch antenna based on the PSEC with a dimension of only $0.107\lambda_0 \times 0.129\lambda_0 \times 0.045\lambda_0$ is then proposed as an example. With the loss and dispersion of the ENG metamaterial layer taken into account, simulated results show the patch antenna has a broadside radiation with radiation efficiency of 84.6%. Compared with the previously proposed counterparts such as the zeroth order resonating antennas and rectangular patch antennas on a juxtaposed DPS-ENG pair, the radiation efficiency of the PSEC or PPSEC based rectangular patch antenna is always guaranteed when the antenna size is reduced, as long as the loss of the ENG metamaterial can be small. Finally some conclusions are given in Section 5.

2. 2-D INFINITELY LONG PARALLEL-PLATE WAVEGUIDE

We start our study with a 2-D parallel-plate waveguide filled with a pair of DPS and ENG metamaterial layers. Its geometry is shown in Figure 1(a). It is assumed that the parallel-plate waveguide is infinitely long in x and y directions and the eigenwaves in this waveguide propagate along y direction, with an $e^{j\omega t}$ time dependence. The parallel-plate waveguide is filled with two layers of substrate. One is a conventional DPS layer, and the other is an ENG metamaterial
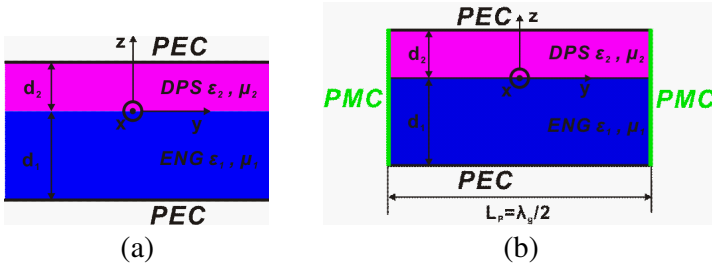
Figure 1. Geometries of (a) a 2-D DPS-ENG bi-layer parallel-plate waveguide, infinitely long in x and y directions. (b) a $\lambda_g/2$ cavity formed by the waveguide terminated by PMC boundaries at both ends.

layer. The permittivity, permeability, and thickness of these two layers are denoted by ε_1, μ_1, d_1 and ε_2, μ_2, d_2, respectively. As for the conventional waveguides and patch antennas, we only discuss the dominant TM surface wave (TM_0) in our study, i.e., the magnetic field has only x component and the electric field has y and z components. The dispersion relation of the TM_0 mode for such a parallel-plate waveguide is [23–25]

$$-\frac{k_{t1}}{\varepsilon_1}\tan(k_{t1}d_1) = \frac{k_{t2}}{\varepsilon_2}\tan(k_{t2}d_2) \tag{1}$$

where $k_{ti} = \sqrt{\omega^2\varepsilon_i\mu_i - \beta^2}$ $(i = 1, 2)$ is the transverse wavenumber of each layer, and β is the longitudinal propagation constant of the surface wave along y direction. It has been shown in [23–25] that with proper constitutive parameters and layer thicknesses of the DPS-DNG (or ENG-MNG) bi-layer waveguide, the slow-wave factor (SWF), defined as the ratio of β and wavenumber of the free space k_0, of the TM_0 surface wave theoretically approaches to infinity toward DC. Here we show that the DPS-ENG (when the DNG layer of the DPS-DNG bi-layer is replaced by an ENG layer) bi-layer waveguide in Figure 1(a) can also support such super-slow TM_0 surface wave. Dispersion relations of this DPS-ENG case, along with the previously reported DPS-DNG case, are plotted in Figure 2(a) for comparison. Because in this section we first concentrate on the possible miniaturization effect at a single specific frequency, we here only consider the ideal case when the ENG and DNG metamaterials are assumed lossless and non-dispersive. The effects of their loss and dispersion will be discussed later in Section 4. One sees in Figure 2(a) that, as the frequency decreases toward DC, the longitudinal propagation constant of the TM_0 surface wave (β) does not approach to zero (β in all three cases are still above $175\,\mathrm{m}^{-1}$ at DC), as that of the TEM wave (k_0) always does in conventional
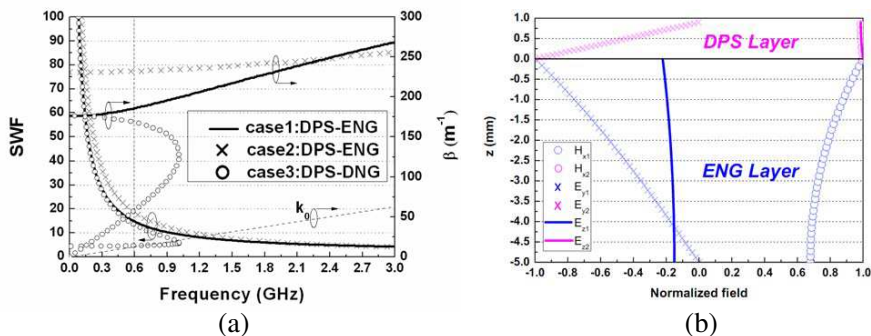
Figure 2. (a) The dispersion relation of the super-slow TM_0 mode in a parallel-plate waveguide in Figure 1(a) filled with a DPS-ENG bi-layer (solid line and crosses) and a DPS-DNG bi-layer (circles). Constitutive parameters of three cases of filling are $\varepsilon_1 = -4.5$, $\mu_1 = 1$, $\varepsilon_2 = 1$, $\mu_2 = 1$ for case 1, $\varepsilon_1 = -1$, $\mu_1 = 0.25$, $\varepsilon_2 = 1$, $\mu_2 = 1$ for case 2, and $\varepsilon_1 = -4.5$, $\mu_1 = -1$, $\varepsilon_2 = 1$, $\mu_2 = 1$ for case 3, respectively. The thickness of two layers are $d_1 = 5\,\text{mm}$ and $d_2 = 0.9\,\text{mm}$ for all three cases. (b) The normalized field distributions in the DPS-ENG bi-layer parallel-plate waveguide of case 1 in (a) at 0.6 GHz.

parallel waveguides. Therefore, the SWF, which physically stands for the degree of miniaturization, increases rapidly at low frequency band and tends to infinity at DC. This provides possibility to design highly miniaturized (below subwavelength) antennas, and other microwave components, with such super-slow wave at low frequencies. We emphasize that such miniaturization neither comes purely from high permittivity of any single layer [1], nor from the phase compensation effect of juxtaposed DPS and metamaterial blocks [16–20]. One can see in Figure 2(a) that similar miniaturization can still be achieved even if both DPS and ENG layers of case 2 have very low absolute value of permittivity. As for the miniaturization, one remarkable advantage of the DPS-ENG bi-layer parallel-plate waveguide discussed in this study over its DPS-DNG bi-layer counterpart is that ENG metamaterial is much easier to practically implement than DNG metamaterial [25, 26].

According to analytical field expressions given in [25], the normalized field distributions of the TM_0 mode in the DPS-ENG bi-layer parallel-plate waveguide at 0.6 GHz, with a corresponding β of $185.745\,\text{m}^{-1}$ and SWF of 14.768 (see case 1 of Figure 2(a)), are plotted in Figure 2(b). One sees that the electric and magnetic field distributions in the waveguide exhibit typical features of a surface wave. It is worth noting that the transverse electric fields (E_z)

have almost constant amplitude in each layer but opposite phase. This distribution of E_z determines the radiation property for such a waveguide-based cavity, which will be discussed in the following section.

3. 2-D CAVITY MODEL OF A $\lambda_g/2$ RESONATOR

It is well-known that a patch antenna can be approximated (for the operation frequency and field distribution in the substrate, etc.) with a theoretical model of a cavity which is bounded by the PEC boundaries (above and below the substrate) and the PMC boundaries along the perimeter of the patch antenna [1]. Note that here PMC only appears in the mathematical model of the cavity, but will not appear in the physical structure of the corresponding patch antenna. Therefore, we try to construct a similar 2-D cavity based on the infinitely long DPS-ENG bi-layer parallel-plate waveguide in Section 2 and evaluate the radiation ability of the corresponding patch antenna.

Similar to the general analysis for conventional cavity resonators, we terminate both ends of the infinitely long DPS-ENG bi-layer parallel-plate waveguide in Section 2 by PMC boundaries (see Figure 1(b)) to form a 2-D $\lambda_g/2$ DPS-ENG bi-layer cavity resonator. The transverse magnetic field (H_x) in the cavity can be obtained with superposition of two traveling waves toward each other, in combination with PMC boundaries ($H_x = 0$) at $y = -L_p/2$ and $y = L_p/2$, and the electric fields in the cavity can then be easily found by the relation of the electric and magnetic fields:

$$\overrightarrow{E_i} = \frac{1}{j\omega\varepsilon_i}\nabla \times \overrightarrow{H_i} \ (i = 1, 2) \tag{2}$$

The magnetic and electric fields of the TM_0 mode in the cavity in the ENG metamaterial layer ($-d_1 < z < 0$) are written as

$$H_{x1} = -j2H_0\cos(k_{t2}d_2)\cos[k_{t1}(z+d_1)]\cos(\beta y)$$

$$E_{y1} = 2H_0\frac{k_{t1}}{\omega\varepsilon_1}\cos(k_{t2}d_2)\sin[k_{t1}(z+d_1)]\cos(\beta y) \tag{3}$$

$$E_{z1} = -2H_0\frac{\beta}{\omega\varepsilon_1}\cos(k_{t2}d_2)\cos[k_{t1}(z+d_1)]\sin(\beta y)$$

and in the DPS layer ($0 < z < d_2$) as

$$H_{x2} = -j2H_0\cos(k_{t1}d_1)\cos[k_{t2}(d_2-z)]\cos(\beta y)$$

$$E_{y2} = -2H_0\frac{k_{t2}}{\omega\varepsilon_2}\cos(k_{t1}d_1)\sin[k_{t2}(d_2-z)]\cos(\beta y) \tag{4}$$

$$E_{z2} = -2H_0\frac{\beta}{\omega\varepsilon_2}\cos(k_{t1}d_1)\cos[k_{t2}(d_2-z)]\sin(\beta y)$$

Here we take the parallel-plate waveguide, filled with the DPS-ENG bi-layer of case 1 ($\varepsilon_1 = -4.5$ and $\varepsilon_2 = 1$) in Figure 2(a), as an example for the following study. As already shown by the solid line in Figure 2(a), the SWF of such waveguide is 14.768 at 0.6 GHz. Thus the physical length (L_p) of the $\lambda_g/2$ DPS-ENG bi-layer cavity is 16.9 mm, which is only $0.0338\lambda_0$. The normalized field distributions of this cavity theoretically predicted by (3) and (4) are plotted in Figure 3(a). One sees that variations of E_z, H_x and E_y along z direction around the central axis ($y = 0$) are similar to those of the infinitely long waveguide (cf., the field distributions of the infinitely long waveguide in Figure 2(b)). To verify these analytical results, we have also conducted an eigenmode analysis of this cavity with the finite element method simulation tool COMSOL Multiphysics [27]. Our simulated results show that the first few resonant frequencies of the TM mode of the cavity are 0.605 GHz, 6.639 GHz, and 14.307 GHz.
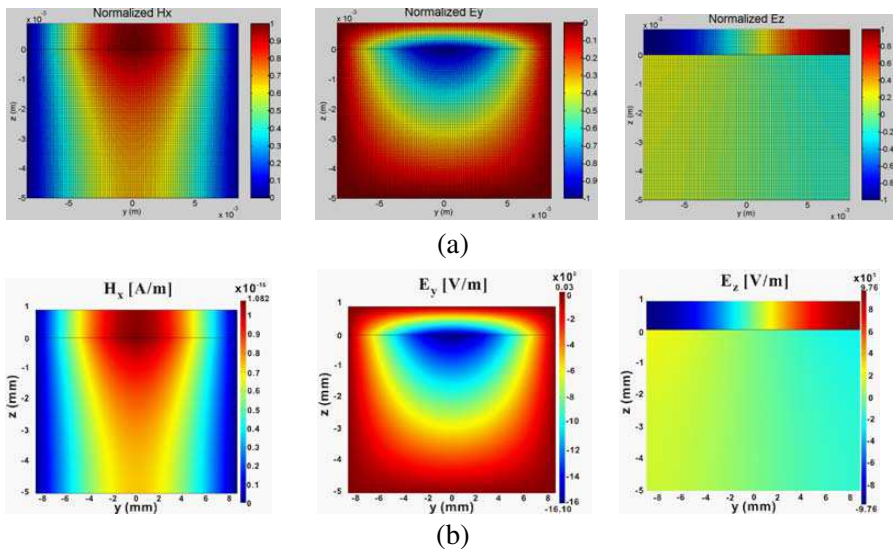

(a)

(b)

Figure 3. The electric and magnetic field distributions for a $\lambda_g/2$ DPS-ENG bi-layer cavity with PEC on the top and bottom and PMC on both ends. Constitutive parameters ($\varepsilon_1 = -4.5$, $\mu_1 = 1$, $\varepsilon_2 = 1$, $\mu_2 = 1$) and thickness ($d_1 = 5$ mm, $d_2 = 0.9$ mm) of the two layers are the same as those of case 1 in Figure 2(a). (a) normalized field distributions calculated from Equations (3) and (4), (b) normalized field distributions calculated with eigenmode analysis in COMSOL Multiphysics.

The resonant frequency of the TM_0 mode (0.605 GHz) predicted by the eigenmode analysis is almost identical with the analytical result (0.6 GHz). Simulated field distributions of the cavity at 0.605 GHz are plotted in Figure 3(b). As expected, the relative amplitude and phase of the field distributions are also consistent (actually identical) to those in Figure 3(a) obtained from analytical Equations (3) and (4).

However, our further simulation shows that the miniaturized cavity in its present form can not be directly used to construct a patch antenna with efficient broadside radiation. The reason is explained as follows. According to the patch antenna theory, the radiation sources of a patch antenna are equivalent magnetic currents at the two edges, each represented by the fringing electric fields $\overrightarrow{E_z}$ as

$$\overrightarrow{M_x} = -2\hat{n} \times \overrightarrow{E_z} \tag{5}$$

where $\hat{n}$ is the normal unit vector of the PMC boundary [1]. Figure 4 illustrates the relation between the fringing electric fields and their equivalent magnetic currents of the cavity.
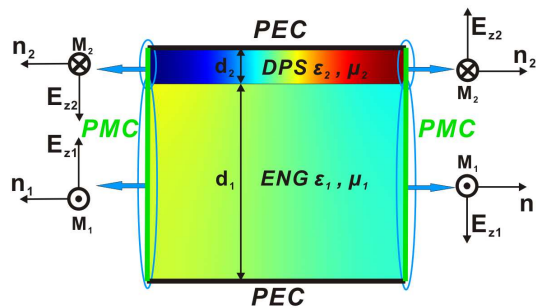

Figure 4. The fringing electric fields and their equivalent magnetic currents for the $\lambda_g/2$ DPS-ENG bi-layer cavity.

One sees that for each layer, the fringing electric fields at two radiating edges are of the same magnitude but out of phase (as mentioned at the end of Section 2), which is also true in the cavity model for a conventional patch antenna and corresponds to a broadside radiation. However, the fringing electric fields in the DPS and ENG layers at the same end are in opposite directions. A simple calculation of the total magnetic current of a single radiating edge shows the total magnetic current of the radiating slot in the ENG layer (M_1) and DPS layer (M_2) are of the same magnitude, but out of phase. When this cavity is used as a radiator, such closely spaced equivalent magnetic currents of the two layers almost cancel each other, and give
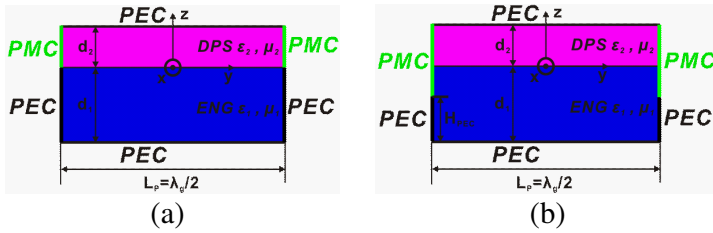
Figure 5. Geometries of (a) a $\lambda_g/2$ DPS-ENG bi-layer cavity with an ENG layer completely shielded by PEC boundary (PSEC), and (b) a $\lambda_g/2$ DPS-ENG bi-layer cavity with an ENG layer partially shielded by PEC boundary (PPSEC). The height of the ENG layer shielded by PEC boundary is H_{PEC}.

no radiation. In other words, this cavity in its present form can not be used directly to construct a patch antenna with efficient radiation.

In order to circumvent this difficulty, we replace (or partially replace) the PMC boundary of one layer (e.g., the ENG layer in our subsequent study) with PEC boundary to form a PEC-Shielded-ENG-Cavity (or PEC-Partially-Shielded-ENG-Cavity). These two cavities are denoted as PSEC and PPSEC for clarity, and their geometries are shown in Figure 5. Since it is hard to perform a rigorous theoretical analysis for these two cavities that are shielded by hybrid boundaries, we only give eigenmode analysis results with COMSOL Multiphysics. The electric and magnetic field distributions for the PSEC, whose constitutive parameters and thickness are identical to case 1 in Figure 2(a), are shown in Figure 6(a). Comparing Figure 6(a) with Figure 3(b), one sees the perturbation of the electric and magnetic fields around the PEC boundaries that shield the ENG layer. As shown in the distribution of E_z in Figure 6(a), E_z at two edges of the ENG layer is zero due to the shielding PEC boundaries. Therefore, when both ends of one layer (the ENG layer in our study) are completely "shielded" by PEC, maximal net equivalent magnetic currents can be obtained, which are only produced by E_z at two radiating edges of the other layer (the DPS layer). Another notable change, when the PMC boundary of the ENG layer is replaced with PEC boundary, is the increase of the TM_0 eigen frequency. The eigen frequency of the PSEC has risen up to 2.49 GHz (the eigen frequency of the original cavity with only PMC boundaries at both ends is 0.6 GHz), thus the electrical length of the PSEC now becomes $0.14\lambda_0$. Although the miniaturization of the PSEC somewhat suffers a lot, the physical length of the cavity is still significantly reduced compared with a conventional $\lambda_0/2$ cavity. More importantly, efficient broadside radiation is inherently
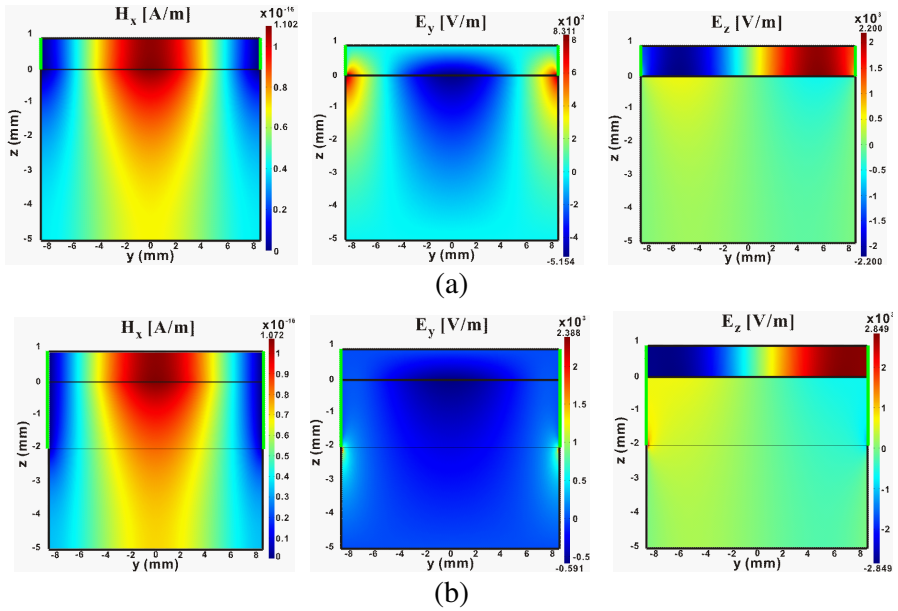
Figure 6. The electric and magnetic field distributions of (a) the PSEC, and (b) the PPSEC. Constitutive parameters and thickness of the DPS and ENG layers in the two cavities are the same as those of the parallel waveguide in Figure 2(a) and the original cavity in Figure 3.
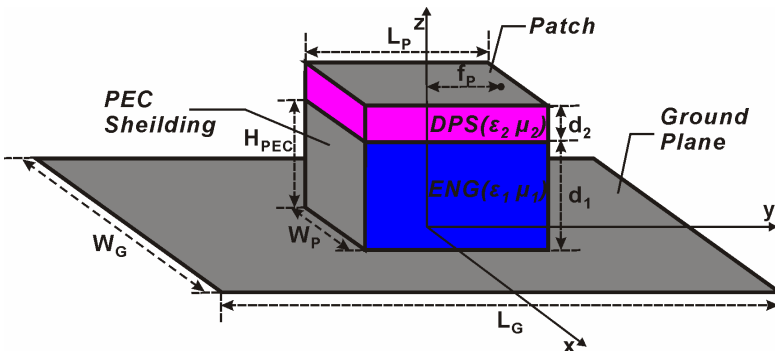

Figure 7. Geometries of a 3-D PSEC-based rectangular patch antenna. Detailed dimensions and constitutive parameters are: $W_G = 100\,\text{mm}$, $L_G = 100\,\text{mm}$, $W_P = 14\,\text{mm}$, $L_P = 16.9\,\text{mm}$, $f_P = 7.5\,\text{mm}$, $d_1 = 5\,\text{mm}$, $d_2 = 0.9\,\text{mm}$, $H_{\text{PEC}} = d_1 = 5\,\text{mm}$, $\varepsilon_1 = -4.5$, $\mu_1 = 1$, $\varepsilon_2 = 1$, $\mu_2 = 1$.

guaranteed in such a PSEC, which will be demonstrated by the full-wave analysis of the PSEC-based patch antenna in Section 4.

Figure 6(b) shows the electric and magnetic field distributions of a PPSEC, when the height of the PEC shielding is $H_{\mathrm{PEC}} = 3\,\mathrm{mm}$. The predicted eigen frequency of this cavity is $1.821\,\mathrm{GHz}$, which is between the eigen frequencies of the original cavity and the PSEC. According to previous analysis, because only part of the ENG layer is shielded by PMC, the net equivalent magnetic current of the PPSEC is less than that of the PSEC, and consequently the radiation will be reduced. This indicates that one can make a trade off between the miniaturization and gain by choosing different H_{PEC}. The dependence of the resonant frequency and radiation properties of the PPSEC-based patch antenna on parameter H_{PEC} will also be discussed in the following section.

4. FULL-WAVE ANALYSIS OF THE PSEC AND PPSEC BASED PATCH ANTENNA

In this section, we use the PSEC and PPSEC to design miniaturized rectangular patch antennas with efficient broadside radiation. Here we first give an example of a PSEC-based rectangular patch antenna, whose geometry is shown in Figure 7. The patch antenna is fed by a simple coaxial probe, whose location is denoted as f_p. One sees that this antenna structure in y-z plane is almost the same as the PSEC except two small differences. One is that the bottom PEC boundary is extended toward both $\pm x$ and $\pm y$ directions as a ground plane. The other is that both ends of the DPS layer of the patch antenna are open-circuited at $y = \pm L_P/2$, instead of the ideal PMC boundary in the PSEC. Such a difference follows from the cavity model for a conventional patch antenna, and the simulated results below will demonstrate the validity of such a substitution. In our study, we always make sure that only TM_0 mode of the surface wave is excited so that fields in the DPS and ENG layers do not vary along x direction (as the case of the 2-D PSEC, which is infinitely long in x direction).

First we still consider the ENG metamaterial layer is lossless and non-dispersive, because this helps quickly determine the accurate resonant frequency of the patch antenna, which is used subsequently as the target of the ENG dispersion specification. The 3-D full wave simulation is conducted with the commercial software CST MICROWAVE STUDIO (CST MWS) [28]. The simulated reflection coefficient is shown in Figure 8 (dashed line). A sole resonance is observed at $2.3\,\mathrm{GHz}$. Best impedance matching ($S_{11} < -25\,\mathrm{dB}$) is achieved after careful optimization of the location of the coaxial feeding probe f_p ($f_p = 7.5\,\mathrm{mm}$, see Figure 7). The electric field distribution
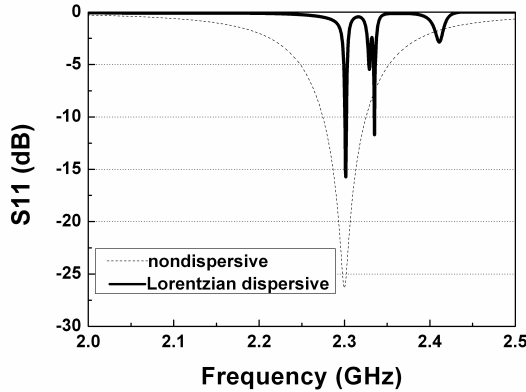
Figure 8. Simulated reflection coefficient of the PSEC-based rectangular patch antenna with non-dispersive and Lorentzian dispersive ENG layer.

on $x = 0$ plane in the DPS and ENG layers of the patch antenna at 2.3 GHz is shown in Figure 9(a). The electric distribution agrees very well with that predicted by the cavity model analysis of the PSEC [cf., E_y and E_z in Figure 6(a)], which also confirms that this resonance (2.3 GHz) of the patch antenna is indeed the super-slow TM_0 mode. The resonance of the patch antenna is 0.19 GHz lower than the prediction (2.49 GHz) of the cavity model. This is, like the case of a conventional patch antenna, associated with an extended length of the patch due to the fringing effect [1].

In order to properly describe the loss and dispersion of the ENG metamaterial, we consider in this paper the general Lorentzian dispersion model [19, 29], which is of almost the same dispersion form (only with slight difference in the numerator [30]) of a wide range of typical ENG metamaterial particles such as electric-LC resonators (ELC) [31] and complementary split ring resonators (CSRR) [32, 33]:

$$\varepsilon_{1r}(\omega) = \varepsilon_\infty + \frac{(\varepsilon_s - \varepsilon_\infty)\omega_0^2}{\omega_0^2 + j\omega\delta - \omega^2} \tag{6}$$

where ω_0 is the resonant frequency and δ is the damping factor. We specify the parameters of the Lorentzian model in such a way that the real part of the relative permittivity of the ENG metamaterial (ε_{1r}) remains -4.5 at 2.3 GHz, exactly as in the earlier non-dispersive case, and the damping factor δ (i.e., the collision frequency) has its magnitude a couple of orders less than the plasma frequency. Therefore, complete parameters of the Lorentzian dispersive models
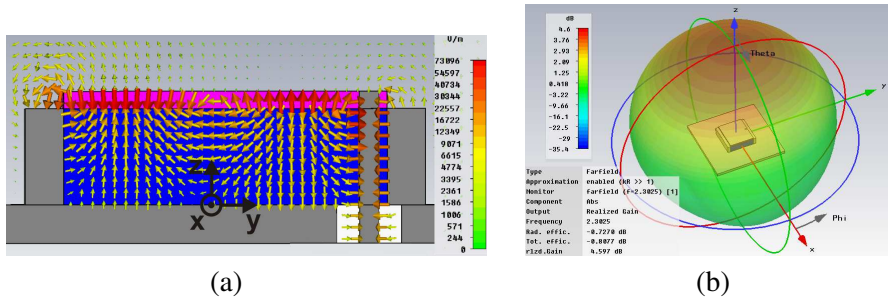
(a)   (b)

Figure 9. Simulated (a) electric field distribution on $x = 0$ plane in the DPS and nondispersive ENG layers and (b) broadside radiation pattern, radiation efficiency, and gain (rlzd. Gain) of the PSEC-based rectangular patch antenna at 2.3025 GHz.

we specified are: $\varepsilon_\infty = 1$, $\varepsilon_s = 4$, $\omega_0 = 1.163 \times 10^{10}$ rad/s, $\delta = 0.5 \times 10^6$ Hz. We also replace all PEC in Figure 7 with copper to include the practical metallic loss. The simulated reflection coefficients are also shown in Figure 8. One sees that for the dispersive models (with real part of ε_{1r} almost the same at 2.3 GHz but different at other frequencies), a resonance with good impedance matching at 2.3025 GHz is still achieved. Compared to the nondispersive case, the fractional impedance bandwidth is reduced a lot and a few unexpected resonances also appear. These are both due to the relatively strong dispersion of the ENG, as the desired TM_0 surface mode cannot be effectively excited but at the very single frequency, and one can hardly guarantee there are no other spurious resonances at near frequencies either. Bandwidth is not the primary concern of this work and it is expected to be improved when elaborate designed particles with very low dispersion is applied during the practical implementation of the ENG metamaterial. The electric field distributions for the Lorentzian dispersive case at 2.3025 GHz are almost the same as those of the non-dispersive case in Figure 9(a), while other spurious resonances are not related to the desired super-slow TM_0 surface mode (not shown for brevity). The radiation properties of the patch antenna with Lorentzian dispersive ENG layer are shown in Figure 9(b). Since the efficient radiation source of this antenna is inherently guaranteed due to the PEC shielding loaded at both radiating edges of the ENG layer, as discussed in Section 3, good broadside radiation with main beam perpendicular to the patch is achieved. Considering the size of the patch antenna is already reduced to a near subwavelength level (only $0.129\lambda_0$), which thus inevitably leads to a rather limited effective

Table 1. Performance of a PPSEC-based patch antenna with lossless and nondispersive ENG layer for different H_{PEC}.

H_{PEC} (mm)	5	4.5	4	3.5	3
f_{cavity} (GHz)	2.490	2.413	2.251	2.049	1.821
f_{antenna} (GHz)	2.300	2.068	1.849	1.673	1.462
L_P/λ_0	0.129	0.116	0.104	0.094	0.082
Directivity (dBi)	5.274	5.008	4.821	4.615	4.336
Radiation efficiency (%)	99.17	92.55	91.58	90.12	88.97
Gain (dBi)	5.230	4.635	4.415	4.159	3.858

radiation aperture (i.e., the two radiating edges of the DPS layer with a height of only $0.007\lambda_0$), the achieved radiation efficiency of 84.6% is fairly good. We stress again that such radiation efficiency is achieved when both metallic and particularly the ENG metamaterial loss of a practical value, have already been taken into account. In fact, with a damping factor of 0.5×10^6 Hz that we specified, the permittivity loss tangent at the resonant frequency is 0.0012, which approaches but still within the lower bound value of practical metamaterials [30].

Besides PSEC, the PPSEC in Section 3, both ends of the ENG layer being only partially shielded by PEC, can also be used to design miniaturized patch antennas. Table 1 shows the resonant frequency of the TM_0 super-slow surface mode of the PPSEC (f_{cavity}), the resonant frequency (f_{antenna}), the electrical dimension (L_P/λ_0) and radiation properties of the PPSEC-based rectangular patch antenna, when we reduce H_{PEC} gradually from 5 mm (the PSEC case). As in this part, the relative variation of the directivity, radiation efficiency and gain, rather than their accurate values, are more concerned, we again use the lossless and non-dispersive ENG metamaterial during the simulation for simplicity. One sees that when H_{PEC} becomes smaller, the boundary condition of the PPSEC is gradually approaching to that of the original cavity in Figure 1(b) and thus the resonant frequency of the PPSEC-based patch antenna can be further reduced, with a deeper miniaturization (below subwavelength). On the other hand, the directivity and gain of the PPSEC-based patch antenna become a bit lower, as the effective area of the antenna further decreases. These results imply that one can make a trade off between the miniaturization and radiation efficiency (gain) by choosing different H_{PEC} when designing a PSEC or PPSEC based rectangular patch antenna, according to the specific requirement of the application.

5. CONCLUSION

The super-slow TM_0 surface wave has been achieved in a DPS-ENG bi-layer parallel-plate waveguide at low frequency band, instead of the previously reported DPS-DNG (ENG-MNG) bi-layer counterpart. It is shown that the cavity model analysis of a $\lambda_g/2$ cavity formed by such a super-slow waveguide verifies its miniaturization, but can hardly provide efficient radiation. This problem is overcome by shielding (or partially shielding) one layer of the cavity at both ends with PEC boundaries. A miniaturized PSEC-based rectangular patch antenna has been designed, with practical loss and dispersion of the ENG metamaterial layer taken into consideration. The antenna has a miniaturized dimension and broadside radiation with fairly good radiation efficiency. The PPSEC-based rectangular patch antenna has also been studied and it has a further miniaturization and reduced radiation efficiency. The main feature of such PSEC or PPSEC based miniaturized rectangular patch antennas is that broadside radiation with good radiation efficiency is inherently guaranteed. This provides a new way of designing compact and low-profile patch antenna elements, planar arrays, waveguide slot arrays, and other compact microwave components.

The work in this paper is a theoretical investigation of potential miniaturization of rectangular patch antennas, based on ideal effective homogeneous bulk metamaterials. The consistency of the results, respectively produced by the analytical predictions, eigenmode analysis and 3-D full wave simulations, confirms their validity for this study. Possible practical implementation of the ENG metamaterial in the future is critical and needs further effort of exploration, as overall properties of the antenna like practical bandwidth and satisfactory radiation efficiency yet await elaborate design of ENG particles (e.g., the CSRR with a planar structure) with extremely low loss and dispersion.

ACKNOWLEDGMENT

REFERENCES

1. Balanis, C. A., *Antenna Theory*, 3rd edition, Wiley, New York, 2005.

2. Garg, R., P. Bhartia, I. Bahl, and A. Ittipiboon, *Microstrip Antenna Design Handbook*, Artech House, Boston, MA, 2001.

3. Xiong, J., Z. Ying, and S. He, "A broadband low profile patch antenna of compact size with three resonances," *IEEE Trans. Antennas Propag.*, Vol. 57, No. 6, 1838–1843, 2009.

4. Sim, Z. W., R. Shuttleworth, M. J. Alexander, and B. D. Grieve, "Compact patch antenna design for outdoor RF energy harvesting in wireless sensor networks," *Progress In Electromagnetics Research*, Vol. 105, 273–294, 2010.

5. Caloz, C. and T. Itoh, *Electromagnetic Metamaterials: Transmission Line Theory and Microwave*, Wiley, New York, 2005.

6. Engheta, N. and R. W. Ziolkowski, *Metamaterials*, Wiley, New York, 2006.

7. Si, L.-M. and X. Lv, "CPW-FED multi-band omni-directional planar microstrip antenna using composite metamaterial resonators for wireless communications," *Progress In Electromagnetics Research*, Vol. 83, 133–146, 2008.

8. Hwang, R.-B., H.-W. Liu, and C.-Y. Chin, "A metamaterial-based *E*-plane horn antenna," *Progress In Electromagnetics Research*, Vol. 93, 275–289, 2009.

9. Pu, T.-L., K.-M. Huang, B. Wang, and Y. Yang, "Application of micro-genetic algorithm to the design of matched high gain patch antenna with zero-refractive-index metamaterial lens," *Journal of Electromagnetic Waves and Applications*, Vol. 24, Nos. 8–9, 1207–1217, 2010.

10. Zhou, H., S. Qu, Z. Pei, Y. Yang, J. Zhang, J. Wang, H. Ma, C. Gu, X. Wang, Z. Xu, W. Peng, and P. Bai, "A high-directive patch antenna based on all-dielectric near-zero-index metamaterial superstrates," *Journal of Electromagnetic Waves and Applications*, Vol. 24, No. 10, 1387–1396, 2010.

11. Montero-de-Paz, J., E. Ugarte-Muñoz, F. J. Herraiz-Martínez, V. González-Posadas, L. E. García-Muñoz, and D. Segovia-Vargas, "Multifrequency self-diplexed single patch antennas loaded with split ring resonators," *Progress In Electromagnetics Research*, Vol. 113, 47–66, 2011.

12. Sanada, A., M. Kimura, L. H. Kubo, C. Caloz, and T. Itoh, "A planar zeroth-order resonator antenna using a left-handed transmission line," *Proceedings of Eur. Microwave Conf.*, 1341–

1344, Amsterdam, The Netherlands, Oct. 2003.

13. Lai, A., K. M. K. H. Leong, and T. Itoh, "Infinite wavelength resonant antennas with monopolar radiation pattern based on periodic structures," *IEEE Trans. Antennas Propag.*, Vol. 55, No. 3, 868–876, 2007.

14. Ziolkowski, R. W. and A. Erentok, "Metamaterial-based efficient electrically small antennas," *IEEE Trans. Antennas Propag.*, Vol. 54, No. 7, 2113–2130, 2006.

15. Erentok, A. and R. W. Ziolkowski, "Metamaterial-inspired efficient electrically small antennas," *IEEE Trans. Antennas Propag.*, Vol. 56, No. 3, 691–707, 2008.

16. Engheta, N., "An idea for thin subwavelength cavity resonators using metamaterials with negative permittivity and permeability," *IEEE Antennas Wireless Propag. Lett.*, Vol. 1, 10–13, 2002.

17. Mahmoud, S. F., "A new miniaturized annular ring patch resonator partially loaded by a metamaterial ring with negative permeability and permittivity," *IEEE Antennas Wireless Propag. Lett.*, Vol. 3, 19–22, 2004.

18. Alù, A., F. Bilotti, N. Engheta, and L. Vegni, "Subwavelength, compact, resonant patch antennas loaded with metamaterials," *IEEE Trans. Antennas Propag.*, Vol. 55, No. 1, 13–25, 2007.

19. Bilotti, F., A. Alù, and L. Vegni, "Design of miniaturized metamaterial patch antennas with μ-negative loading," *IEEE Trans. Antennas Propag.*, Vol. 56, No. 6, 1640–1647, 2008.

20. Chen, P. Y. and A. Alù, "Sub-wavelength elliptical patch antenna loaded with μ-negative metamaterials," *IEEE Trans. Antennas Propag.*, Vol. 58, No. 9, 2909–2919, 2010.

21. Xiong, J., H. Li, Y. Jin, and S. He, "Modified TM_{020} mode of a rectangular patch antenna partially loaded with metamateria for dual-band applications," *IEEE Antennas Wireless Propag. Lett.*, Vol. 8, 1006–1009, 2009.

22. He, S., J. Xiong, H. Li, and Y. Jin, "Patch antennas based on a pair of DPS and SNG metamaterial," *2010 Proceedings of the Fourth European Conference on Antennas and Propagation (EuCAP), Microwave Conf.*, 1–3, Barcelona, Spain, Apr. 2010.

23. Nefedov, I. S. and S. A. Tretyakov, "Theoretical study of waveguiding structures containing backward-wave materials," *XXVII International Union of Radio Science Gen. Assembly*, 1–3, Maastricht, The Netherlands, Apr. 2010.

24. Nefedov, I. S. and S. A. Tretyakov, "Waveguide containing a backward-wave slab," *Radio Sci.*, Vol. 38, No. 6, 1101–1110, 2003.

25. Alù, A. and N. Engheta, "Guided modes in a waveguide filled with a pair of single-negative (SNG), double-negative (DNG), and/or double-positive (DPS) layers," *IEEE Trans. Microw. Theory Tech.*, Vol. 52, No. 1, 199–210, 2004.

26. Alù, A., N. Engheta, A. Erentok, and R. W. Ziolkowski, "Single-negative, double-negative and low-index metamaterials and their electromagnetic application," *IEEE Trans. Antennas Propag.*, Vol. 49, No. 1, 23–36, 2007.

27. http://www.comsol.com.

28. CST MWS. Comput. Simulation Technol., Darmstadt, Germany, [Online]. Available: http://www.cst.com.

29. Sabah, C. and S. Uckun, "Multilayer system of Lorentz/Drude type metamaterials with dielectric slabs and its application to electromagnetic filters," *Progress In Electromagnetics Research*, Vol. 91, 349–364, 2009.

30. Cummer, S. A., B. Popa, and T. H. Hand, "Q-based design equations and loss limits for resonant metamaterials and experimental validation," *IEEE Trans. Antennas Propag.*, Vol. 56, No. 1, 127–132, 2008.

31. Schurig, D., J. J. Mock, and D. R. Smith, "Electric-field-coupled resonators for negative permittivity metamaterials," *Appl. Phys. Lett.*, Vol. 88, 041109, 2006.

32. Falcone, F., T. Lopetegi, M. A. G. Laso, J. D. Baena, J. Bonache, M. Beruete, R. Marqués, F. Martín, and M. Sorolla, "Babinet principle applied to the design of metasurfaces and metamaterials," *Phys. Rev. Lett.*, Vol. 93, No. 19, 197401, 2004.

33. Zhang, Q.-L., W.-Y. Yin, S. He, and L.-S. Wu, "Evanescent-mode substrate integrated waveguide (SIW) filters implemented with complementary split ring resonators," *Progress In Electromagnetics Research*, Vol. 111, 419–432, 2011.